International Journal of Adhesion & Adhesives 31 (2011) 695–703

Contents lists available at ScienceDirect

International Journal of Adhesion & Adhesives

journal homepage: www.elsevier.com/locate/ijadhadh

Mode-I adhesive fracture energy of carbon fibre composite joints with nanoreinforced epoxy adhesives

M.R. Gude*, S.G. Prolongo, T. Gómez-del Río, A. Ureña

Department of Materials Science and Engineering, University Rey Juan Carlos, c/ Tulipán s/n, 28933 Móstoles, Madrid, Spain

ARTICLE INFO

Article history:
Accepted 20 June 2011
Available online 1 July 2011

Keywords:
Epoxy
Composites
Surface treatment
Fracture mechanics
Nanocomposites

ABSTRACT

The effect of the addition of carbon nanoreinforcements to an epoxy adhesive on the strength and toughness of carbon fibre/epoxy composite joints was studied. The laminate surfaces, treated with peel ply, were characterised by profilometry, image analysis and wettability. The mechanical properties of the joints were determined by lap shear testing and double cantilever beam testing. The fracture mechanisms were studied by scanning electron microscopy.

The addition of carbon nanofibres and carbon nanotubes caused an increase in the mode-I adhesive fracture energy, G_{IC}, of the joints while their lap shear strengths remained approximately constant. This improvement in the fracture behaviour was attributed to the occurrence of toughening mechanisms when carbon nanoreinforcements were added to the epoxy adhesive. Additionally, the use of carbon nanotubes improved the interfacial strength between the adhesive and the substrate, changing the crack growth behaviour and the macroscopic failure mode.

1. Introduction

Carbon fibre/epoxy laminates are widely used composite materials in fields such as the automotive and aerospace industries, energy production and sports equipment. In many of these applications, the large size and complexity of the structures require the use of joining techniques to assemble various parts. These joints can be made either mechanically or using adhesives. In the case of carbon fibre reinforced polymers (CFRPs), adhesive bonding presents many advantages compared with the use of mechanical joints [1]. Among others, bonding does not require drilling holes in the substrates and allows for the joining of large surfaces. Adhesive joints also minimise stress concentrations, distributing the load over the overlapping area. One of the main limitations of adhesive joints is the need for applying a surface treatment to the adherends to promote their adhesion [2]. Due to the novelty of this method, the efficiency of each particular joint must be analysed, and new formulations of adhesives with improved properties must be developed.

Epoxy resins are one of the most important structural adhesives due to their good adhesive properties and high thermal and chemical resistance. When joining carbon fibre/epoxy composites, epoxy adhesives have a high compatibility with the matrix. The main limitations of epoxies are their low fracture toughness and very high electrical resistivity. This last is a disadvantage in some applications of carbon fibre/epoxy structures in which electrical conductivity is desired throughout the structure. This requirement cannot be fulfilled if different parts are joined using an insulating material such as epoxy. To increase the toughness of epoxy resins, one of the most commonly used solutions is the addition of polymeric particles. However, the increase in fracture toughness is at the expense, in many cases, of detrimental effects on other properties [3,4]. Recently, the use of nanometric particles as epoxy additives has been investigated. Gilbert et al. [5] achieved an important enhancement of the mode-I fracture toughness of co-cured CFRP joints by adding alumina nanoparticles to the adhesive. However, when the laminates were previously cured, fracture toughness values obtained were even lower than those with unreinforced adhesive. Moreover, this kind of nanoparticle does not solve the problem of low electrical conductivity.

It has been reported that the introduction of carbon nanotubes (CNTs) or nanofibres (CNFs) can improve the mechanical, thermal and electrical properties of epoxy resins [6–9]. The most common problems found during the processing of epoxy nanocomposites are associated with the difficulties of obtaining both a suitable dispersion of nanoreinforcements and a high interaction with the matrix. Several of these issues were partially solved in our previous work [10], where a dispersion method based on the use of a solvent and ultrasonication was optimised. With this method, it was possible to obtain a good dispersion of nanoreinforcements in epoxy resins with contents up to 0.5 wt% CNFs

* Corresponding author. Tel.: +34 91 488 80 83; fax: +34 91 488 81 50.
E-mail address: maria.gude@urjc.es (M.R. Gude).

0143-7496/$ - see front matter © 2011 Elsevier Ltd. All rights reserved.
doi:10.1016/j.ijadhadh.2011.06.016

and 0.25 wt% CNTs, as determined by TEM [11]. Higher percentages induced a very high increase in resin viscosity, which made it more difficult to use the filled epoxy resins as adhesives. The maximum content for proper dispersion is lower for CNTs than CNFs because of their higher specific surface area, which increases the viscosity of the mixtures more than the same weight percentage of CNFs [11]. Several researchers have demonstrated that low contents of CNTs yield better property improvements than higher contents of CNFs due to the excellent mechanical, electrical and thermal characteristics of CNTs [12–14]. In our laboratory, we found that the addition of 0.1 wt% CNTs and 0.25 wt% CNFs caused reductions in the electrical resistivity of 13 and 10 orders of magnitude, respectively, compared with the neat epoxy adhesive [11].

The use of these nanoreinforced adhesives for joining carbon fibre/epoxy composites was also researched in our previous work [11], in which we found that the addition of nanoreinforcements did not significantly affect the lap shear strength of single lap joints. However, some changes were observed in the fracture surfaces of these joints, which may indicate an increase in the fracture toughness. This led us to study the adhesive fracture energy in an effort to determine if the presence of CNFs or CNTs can modify the fracture toughness of carbon fibre composite joints.

In the present work, we evaluated the viability of the addition of CNFs and CNTs to epoxy adhesives for joining carbon fibre/epoxy laminates. The objective was to increase the toughness of the joints through the formation of new micromechanical mechanisms associated with the presence of nanoreinforcements that contribute to the increase in energy consumption during fracture.

2. Experimental

2.1. Materials

The unidirectional carbon fibre/epoxy laminates used as adherends were manufactured by the Instituto Nacional de Técnica Aerospacial (Spain) from unidirectional prepregs (Hexply 8552/34%/UD134/AS4-12K, supplied by Hexcel (Stamford, USA)) laid up and then cured in an autoclave. The matrix of this prepreg is an amine-cured, toughened epoxy resin designed for use in primary aerospace structures. The nominal fibre volume is 57%. The curing was performed at 180 °C for 2 h at a pressure of 6 bar. Before curing, a dry polyester peel ply (Release Ply C, Airtech (Differdange, Luxembourg)) was placed over the last prepreg. This ply was removed just before bonding, to generate a rough surface free of contamination. Both the peel-ply-treated surface and the untreated composite surface were characterised by roughness and surface free energy measurements. The smooth surface without peel ply was simply wiped with acetone.

The epoxy monomer used was the diglycidyl ether of bisphenol A (DGEBA), with 178 g/epoxy equivalent. The curing agent was 4,4′-diaminodiphenylmethane (DDM). Both components of the epoxy adhesive were supplied by Sigma–Aldrich. Carbon nanofibres (CNFs) and carbon nanotubes (CNTs) were used as reinforcements in this adhesive. The CNFs, manufactured by Grupo Antolín, were produced by chemical vapour deposition. Their average diameter depends on their morphology: for platelet-like CNFs, it is from 12–20 nm, whereas cup-stacked CNFs have diameters less than 93 nm [15]. According to the manufacturer, their lengths are estimated to be greater than 30 μm. Amino-functionalised multiwall carbon nanotubes, with diameters less than 10 nm and lengths below 1 μm, were produced by Nanocyl via catalytic carbon vapour deposition. As specified in the datasheet of this product (Nanocyl 3152), the extent of functionalisation is less than 0.5%, as measured by X-ray photoelectron spectroscopy (XPS).

To achieve a good dispersion of CNFs and CNTs in the adhesive, the processing of nanoreinforced adhesives was performed in several steps. This process includes the use of chloroform and several dispersion techniques, and has been optimised in a previous work [10]. The CNF content was 0.5 wt% with respect to the mass of DGEBA. In the case of the CNTs, only 0.25 wt% was added because of their greater effect on the viscosity increase due to their high specific surface area. Additionally, these percentages of nanofillers were chosen because they provided the highest values of lap shear strength in a previous study performed with different surface treatments of the substrates [11,16]. The curing process for the neat and reinforced adhesives was performed in two steps: 3 h at 150 °C and then 1 h at 180 °C.

2.2. Characterisation

The surfaces of the carbon fibre/epoxy laminates used as adherends were treated with peel ply and then characterised by profilometry (Mitutoyo Surftest SJ-301) and image analysis using Scanning Probe Image Processor (SPIP) software [17] to determine their surface textures. The surface free energy of the adherends was determined from the contact angles of water and glycerol, measured with a Ramé-Hart 200 contact angle goniometer. Five drops of each liquid were placed on each composite sample using a microsyringe, and ten measurements of the contact angle were made, at the left and right sides of every drop, with a precision of 0.1°. There are several methods for calculating surface energy using the contact angles of different liquids. In the absence of complete consensus regarding which of them is most suitable for measuring polymer surface energies, and taking into account other studies focusing on the same materials [18–20], the equation proposed by Owens and Wendt [21], also known as the OWRK (Owens, Wendt, Rabel and Kaelble) equation, was chosen to calculate the dispersive and polar fractions of the surface energy

$$\sigma_l(1+\cos\theta)=2\sqrt{\sigma_s^D\sigma_l^D}+2\sqrt{\sigma_s^P\sigma_l^P}$$

where σ_s and σ_l correspond to the surface free energy of the adherend and the surface tension of the liquid, respectively, and the superscripts D and P correspond to the dispersive and polar fractions, respectively. The contact angles, θ, of the adhesives on both surfaces (untreated and peel-ply-treated) were also measured, and these data were used to calculate their surface tensions. In this case, the mean and standard deviations were calculated from ten measurements of the contact angles of three drops per adhesive.

The joint strength was determined by single lap shear tests according to the ASTM standard D5868. The adherends were 100 mm long, 25 mm wide and 2.5 mm thick. The area of the overlap was 25×25 mm^2, and the adhesive thickness was 0.7 mm. Five tests were done for each adhesive composition.

Double cantilever beam (DCB) tests were performed to determine the mode-I adhesive fracture energy of the adhesive joints, following the protocol "Determination of the Mode-I Adhesive Fracture Energy, G_{IC}, of Structural Adhesives using the Double Cantilever Beam (DCB) and Tapered Double Cantilever Beam (TDCB)" [22]. In this case, the adherends were 150 mm long, 25 mm wide and 3.3 mm thick. A 75 μm thick polyethylene terephthalate (PTFE) film was inserted at one end of the specimen to act as a crack initiator. To perform the test, a precrack was generated from the nonadhesive insert, and then the DCB test was performed. The thickness of the adhesive was 0.4 mm. To

facilitate the detection of crack growth, one edge of the sample was coated with a thin layer of typewriter correction fluid. In the DCB testing, the load was applied to the specimens at a constant cross-head rate of 1 mm/min. The measured displacement, δ, was corrected with the system compliance. Blackman et al. [23] demonstrated the importance of this correction. Five samples were tested for each adhesive composition. Fig. 1 shows two typical load–displacement curves obtained during the testing: (a) the crack progresses continuously and (b) unstable "stick-slip" crack growth behaviour.

For the calculation of the mode-I strain energy release rate, G_{IC}, three different methods were employed

1. Corrected beam theory (CBT) [22]

$$G_{IC} = \frac{3P\delta}{2B(a+|\Delta|)}\frac{1}{N}$$

where P is the load, δ is the displacement, a is the crack length (measured from the load line) and B is the width of the specimen. The factor Δ is used to correct the error produced when the beam is not perfectly built-in, treating it as containing a slightly longer crack length ($a+|\Delta|$). The value of Δ may be determined experimentally by plotting the cube root of the normalised compliance $(C/N)^{1/3}$ as a function of crack length a. The compliance C is the ratio between displacement and load (δ/P). The extrapolation of a linear fit of the plotted data yields Δ as the intersection point with the abscissa (see Fig. 2a). N is a correction factor applied because load blocks were used to apply the load to the specimen, and is calculated using the following equation:

$$N = 1-\left(\frac{l_2}{a}\right)^3-\frac{9}{8}\left[1-\left(\frac{l_2}{a}\right)^2\right]\frac{\delta l_1}{a^2}-\frac{9}{35}\left(\frac{\delta}{a}\right)^2$$

where l_1 is the distance from the centre of the loading pin to the midplane of the arm of the substrate beam and l_2 is the horizontal distance from the loading pin centre to the edge of the block.

2. Experimental compliance method (ECM) [22]

$$G_{IC} = \frac{nP\delta}{2Ba}\frac{1}{N}$$

where P, δ, a, B and N are the same as in the corrected beam theory and n is the slope of the plot of the logarithm of the normalised compliance (C/N) versus the logarithm of the crack length a (Fig. 2b).

3. Area method [24]

$$G_{IC} = \frac{A}{(b-a)B}$$

where A is the area under the P–δ curve between two points, a and b, obtained as shown in Fig. 3, $(b-a)$ is the length of the crack between two points on the specimen and B is the width of the specimen. The last method provides a mean value, whereas the first two allows for the determination of the resistance curve (R-curve), which is a graph of the propagation values of the adhesive fracture energy G_{IC} versus crack length.

The fracture surfaces of the adhesive joints were examined by scanning electron microscopy (SEM Hitachi S3400N) and field

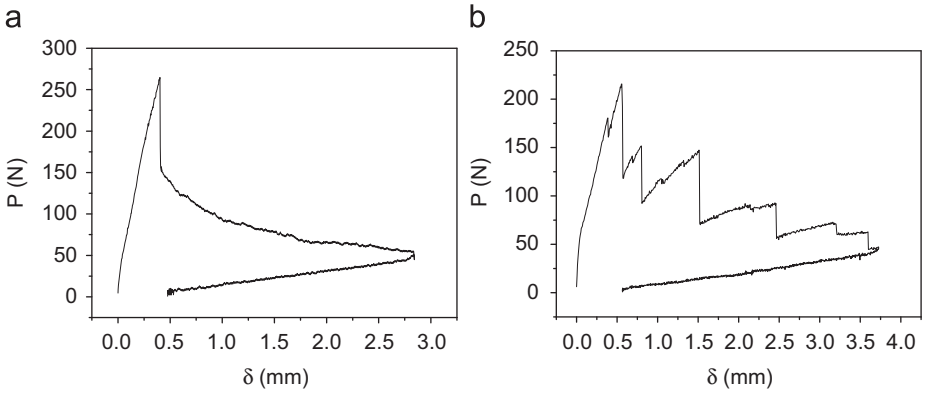

Fig. 1. Load–displacement curves obtained in the DCB, where the crack progressed continuously with neat epoxy adhesive (a) and exhibited unstable "stick-slip" crack growth behaviour with epoxy/CNT adhesive (b).

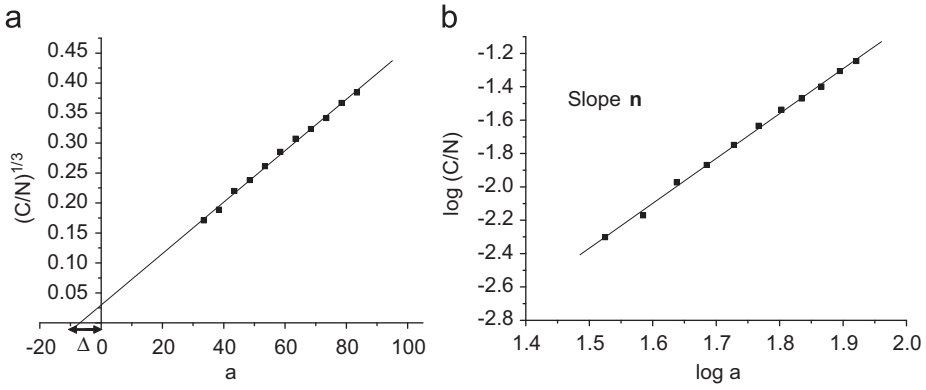

Fig. 2. Linear fits used to determine the parameters Δ (a) and n (b).

emission scanning electron microscopy (FEG-SEM Nova NanoSEM FEI 230) after coating with a 5–10 nm Au–Pd layer by sputtering.

3. Results and discussion

3.1. Surface roughness

It is well known that surface topography plays an important role in adhesion because pits, valleys, peaks and other types of topographical features on the surfaces of adherends can provide additional surface area for bonding and allow for mechanical interlocking to take place between the substrate and adhesive, enhancing adhesion [1,25]. Conversely, surfaces with very high peaks or deep holes may allow air to be trapped at the interface, creating stress concentrations in the interface region of the bond and reducing adhesion.

As expected, the profile obtained for the peel-ply-treated laminate was extremely jagged and rough, showing peaks and valleys in a regular pattern. The average roughness, R_a, measured with the profilometer was 6.7 μm, with a standard deviation of 0.1 μm (6.7 ± 0.1 μm). This is a high value compared with the roughness obtained for the untreated laminate of 0.26 ± 0.02 μm. This parameter alone is insufficient to fully characterise the texture of a surface; two surfaces with similar average roughnesses can present very different surface textures. For this reason, a wide range of roughness parameters have been defined. The image analysis software SPIP can be used to analyse not only lines but surfaces, and this allows the determination of various parameters that together better define the texture of a surface. Fig. 4 shows the analysed low-magnification SEM micrographs captured and the 3D reconstruction of the surface generated using the image analysis software. Through this analysis, we determined that the increase in available area for bonding compared with a flat surface was approximately 6500% for the peel ply and 2200% for the untreated laminates. This was mainly caused by the increased height of the peaks and depth of the valleys, defined as R_z (peak–peak height: the average height of the five highest local maxima plus the average depth of the five lowest local minima), which was 1.6 μm for the untreated surface and considerably higher for the composite treated with peel ply (33.8 μm). The SPIP analysis also allowed us to determine the summit densities (S_{dq}, the number of local maxima per unit area), which were 0.047 and 0.012 μm^{-2} for the untreated and peel-ply-treated surfaces, respectively, meaning that the latter had fewer peaks, and consequently, the distance between them was greater. The height of the peaks in the peel-ply-treated adherends could cause problems with trapped air if they were very close together, but this was avoided in our case due to the large distance between peaks.

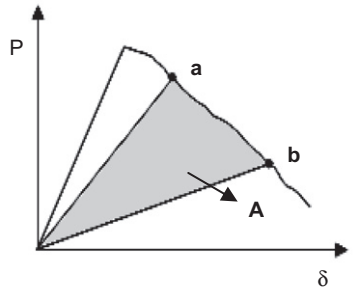

Fig. 3. Area used for the calculation of G_{IC} following the area method.

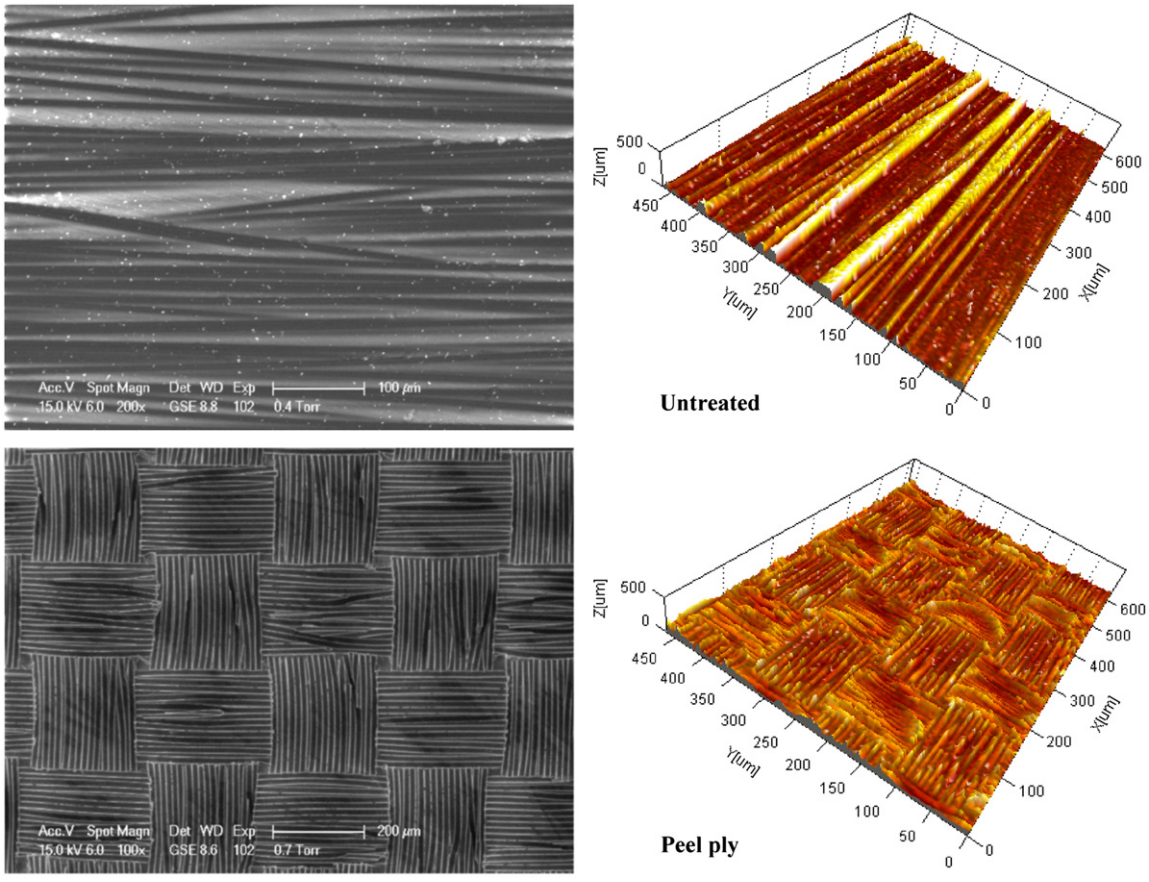

Fig. 4. Image analysis of SEM micrographs of untreated and peel-ply-treated surfaces.

Table 1
Mean values and standard deviations of the surface free energies of the adherends and the contact angles of the adhesives.

	Surface free energy (mJ/m^2)			Contact angle (deg.)		
	Dispersive	Polar	Total	DGEBA	DGEBA/CNF	DGEBA/CNT
Untreated	8.5 ± 1.5	19.3 ± 2.0	27.8 ± 0.6	49.3 ± 1.9	38.5 ± 1.7	49.5 ± 3.0
Peel ply	29.8 ± 1.8	6.6 ± 0.9	36.4 ± 1.0	34.1 ± 2.7	39.6 ± 1.8	38.8 ± 3.9

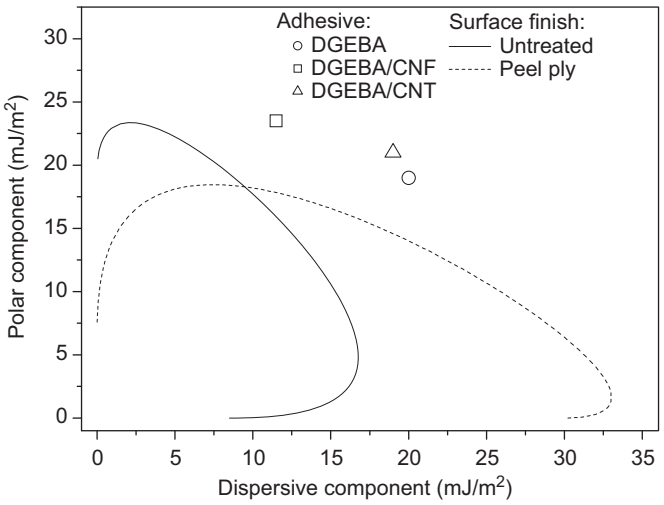

Fig. 5. Wetting envelope of the untreated and peel-ply-treated adherends and surface tensions of the adhesives.

3.2. Surface energy and wetting

In addition to the surface roughness, the surface free energy is a characteristic that determines the adhesive properties of the adherends. As explained in Section 2.2, this energy was determined from contact angle measurements of two liquids, i.e., water and glycerol, using the method of Owens and Wendt [21]. Table 1 lists the dispersive and polar components of the surface free energies and the wettabilities of the uncured adhesives on the two studied surface finishes.

The dispersive component of the surface free energy is related to the surface roughness. We observed that R_a, R_z and σ_s^D were very low for the untreated adherends, having very flat surfaces, and considerably higher for the peel-ply-treated adherends. In fact, the surface areas and the dispersive surface energies for these laminates were both approximately three times that of the corresponding untreated laminates. The polar component was relatively high for the untreated surface. In principle, this is a desirable characteristic; however, for untreated surfaces, this phenomenon is usually due to the presence of contaminants or water. In contrast, peel-ply treatment generates a surface free of contamination, characterised by a low number of polar groups as well as high roughness. As observed by other researchers, the surface treatment of carbon fibre/epoxy composites with polyester peel plies induces the predominance of apolar groups, increasing the dispersive component of the surface energy [2].

Based on these data and the OWRK equation, the wetting envelopes were calculated. These curves are the geometric spaces of the liquids, represented by their polar and dispersive surface tensions, that wet the surface with a given contact angle. For an angle of 0°, this curve represents the critical surface tension for complete wetting (Fig. 5). Liquids situated inside this envelope completely wet the surface, whereas liquids situated outside the wetting envelope, due to their dispersive and polar surface tension, wet the surface with a contact angle greater than 0°. Thus, for a given surface finish, the wettability is better when the liquid is closer to the wetting envelope. This means that the adhesives more effectively wet the surfaces of the peel-ply-treated laminates than the untreated adherends. This result was expected because the surface free energy of the peel-ply-treated laminates is higher. However, it has been observed that liquids with certain combinations of surface tension components (i.e., high σ_l^P and low σ_l^D) better wet the untreated laminates. This indicates that wetting depends not only on the surface free energy of the substrate and the surface tension of the liquid but also on how the dispersive and polar components of each are distributed.

As mentioned, wetting envelopes may also be calculated for different contact angles, not only the complete wetting (0°), using the OWRK equation. Outside of a particular wetting envelope, the contact angle is higher than that represented by the envelope, and the contact angle is lower inside the envelope. This allows the estimation of the contact angle of a liquid of known surface tension by plotting the contours for different contact angles. In this case, the surface tension of the adhesives was unknown and was calculated from their contact angles on untreated and peel-ply-treated adherends and the OWRK equation. As expected, the contact angles between the adhesives and the adherends predicted in Fig. 6 agreed with the experimental values. The surface tensions of the three adhesives were quite similar: 39, 35 and 40 mJ/m^2 for DGEBA, DGEBA/CNF and DGEBA/CNT, respectively. For the neat and CNT-reinforced adhesives, both components of the surface tension are practically equal. However, with CNF addition, the surface tension of the adhesive became mainly polar. This explains why this adhesive better wet the untreated composite. However, the addition of carbon nanofibres had the converse effect on the peel-ply-treated surface, reducing the wettability by a few degrees compared with the neat adhesive. In general, the addition of carbon nanoreinforcements did not significantly change the wetting behaviour of the adhesives, and peel-ply treatment improved this behaviour.

Summarising the surface characterisation, peel-ply treatment, compared with the untreated laminates, provided a surface free of contamination, with high roughness despite the low number of peaks and valleys, and produced a considerable increase in the surface area available for bonding. This treatment also caused a decrease in the polar component and increased the dispersive component, resulting in an increase in the surface free energy of the composite. Combining the surface energies of the surfaces and the adhesives, the wetting envelopes demonstrated that adhesives better wet the peel-ply-treated laminates than the untreated laminates. This justified the selection of this treatment for the adhesive joints that were studied subsequently.

3.3. Properties of adhesive joints

Adhesive joints with two different geometries were manufactured to determine the adhesive strength (lap shear joints) and the mode-I adhesive fracture energy (double cantilever beam joints) in laminates treated with peel ply. The lap shear strength

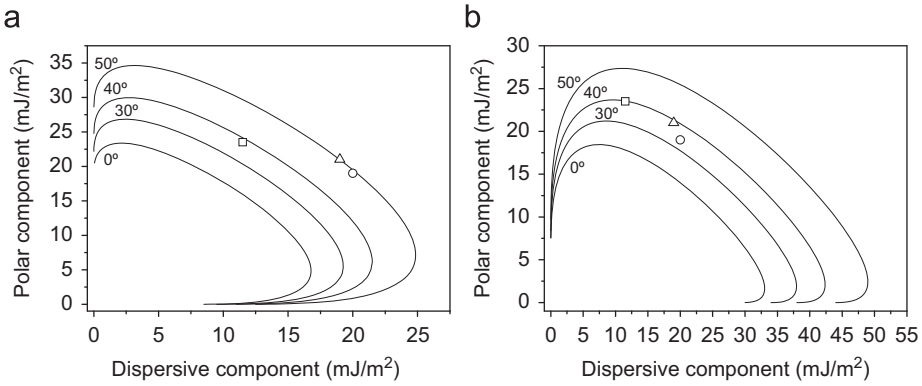

Fig. 6. Wetting envelopes with 0°, 30°, 40° and 50° contours for the untreated (a) and peel-ply-treated (b) adherends. The surface tensions of the uncured adhesives are also represented: ○ DGEBA, □ DGEBA/CNF, Δ DGEBA/CNT.

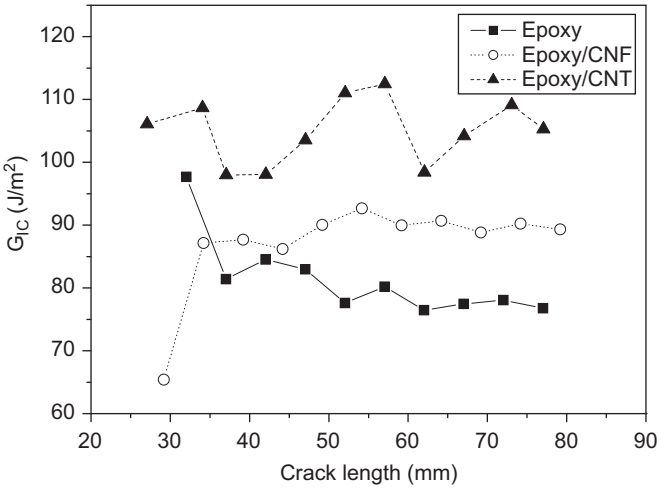

Fig. 7. *R*-curves calculated using CBT for DCB joints with the different adhesives.

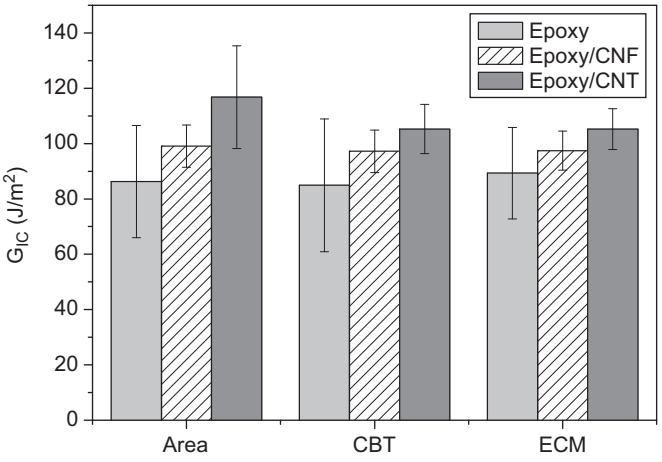

Fig. 8. Comparison of the mean propagation values and standard deviation of G_{IC} as a function of the adhesive composition and the calculation method.

had a mean value of 8.6 MPa with a standard deviation of 0.6 MPa for the adhesive joints with neat epoxy adhesive, 9.2 ± 0.7 MPa for the adhesive reinforced with 0.5 wt% CNFs and 9.2 ± 0.6 MPa for the adhesive with 0.25 wt% CNTs.

Thus, the addition of carbon nanofibres or carbon nanotubes to epoxy adhesive did not significantly change the bond strength. However, as reported in a previous work [11], the presence of these nanoscale fillers caused the appearance of new mechanisms of adhesion. The fracture failure was adhesive in all cases, but in the joints with nanoreinforced adhesive, there were some small areas of cohesive failure in the adherend [11]. This small change in the failure mechanism could indicate a change in the fracture toughness values of the adhesive joints when carbon nanofillers were added to the epoxy adhesive. The results of the DCB tests described herein confirmed this hypothesis.

The three calculation methods described in Section 2.2 were applied to each DCB-tested joint. The area method provided a G_{IC} value for each joint. The arithmetic mean and standard deviation were calculated for each adhesive composition using the five values of the mode-I adhesive fracture energy corresponding to the five joints tested. Using CBT and ECM, G_{IC} was calculated for each measured crack length (between 5 and 60 mm of crack propagation from the precrack, every 5 mm). Fig. 7 shows one *R*-curve per adhesive composition using the G_{IC} values calculated with the corrected beam theory. For the epoxy and epoxy/CNF adhesives, cracks progressed continuously (Fig. 1a), and the G_{IC} did not change significantly as a function of the crack length.

Table 2
Mean G_{IC} values and standard deviations for the different adhesives using three calculation methods.

Adhesive	Calculation method		
	Area	CBT	ECM
Epoxy	86.3 ± 20.3	87.0 ± 26.4	92.1 ± 18.7
Epoxy/CNF	99.1 ± 7.7	96.0 ± 8.7	96.7 ± 8.2
Epoxy/CNT	116.8 ± 18.6	105.3 ± 8.9	105.3 ± 7.4

Table 3
Failure modes of DCB joints.

Adhesive	Macroscopic failure mode	
	Adhesive (%)	Cohesive (%)
Epoxy	100	–
Epoxy/CNF	100	–
Epoxy/CNT	80	20

However, the addition of CNTs to the epoxy adhesive promoted a change in the crack growth to a "stick-slip" behaviour (Fig. 1b). This caused variability in the G_{IC} values for each crack length. An average value of G_{IC} was obtained from each DCB joint tested using CBT and ECM from the *R*-curves. The average values and standard deviations, shown in Fig. 8 and Table 2, were then

calculated using the average value of the five joints tested per adhesive. Although the standard deviation was quite high in some cases, the mean G_{IC} values indicate that the addition of carbon nanoreinforcements to the adhesive increased the fracture energy of the DCB joints. This was deduced independently of the calculation method used. In general, the mean values of each adhesive were very similar, again independently of the method used for their calculation.

The reinforcement of epoxy adhesives with carbon nanofibres increased the mode-I fracture energy of DCB joints of the carbon fibre/epoxy laminates by 10% over the neat adhesive, and the increase with the addition of carbon nanotubes was 23.5%. To explain these results, the failure modes of the joints were analysed both macro- and microscopically. In all of the tested joints with neat and CNF reinforced adhesives, the failure was found to be macroscopically adhesive, as can be seen in Table 3 and Fig. 9a and b. However, the samples bonded with CNT/epoxy adhesive broke in a mixed adhesive/cohesive mode within the adhesive. As shown in Fig. 9c, the crack moved from one adhesive/adherend interface to the opposite interface by propagating through the adhesive layer. This could indicate that carbon nanotubes improved the interface between adhesive and substrate, preventing the crack propagating along the interface and causing "stick-slip" crack growth behaviour. This resulted in an increase in the mode-I adhesive fracture energy. The resultant failure mode was mainly adhesive, with a proportion of cohesive failure (Table 3). This could also explain the higher value of G_{IC} calculated by the area method than the values given by the CBT and ECM methods. This difference demonstrates that the area method is the least accurate of the three methods used, particularly when crack growth shows "stick-slip" behaviour. This observation is especially interesting from a practical point of view, as it provides an average value quite similar to those obtained with the other two methods (in the worst case, the difference was approximately 10%) but with easier and quicker calculations.

The fracture surfaces were studied in depth using scanning electron microscopy (SEM) and field emission gun-SEM (FEG-SEM) to determine the role played by the nanoreinforcements in increasing the adhesive fracture energy. In the initiation zone, the fracture surfaces showed that the joint broke in a brittle mode. However, in the joints with nanoreinforced adhesives, there were more signs of microfibrillation, which is a typical mechanism of energy consumption during the fracture of epoxy resins.

The micrographs of the propagation zone (Figs. 10–12) corresponded in all cases to the side of the joint with adhesive. At low

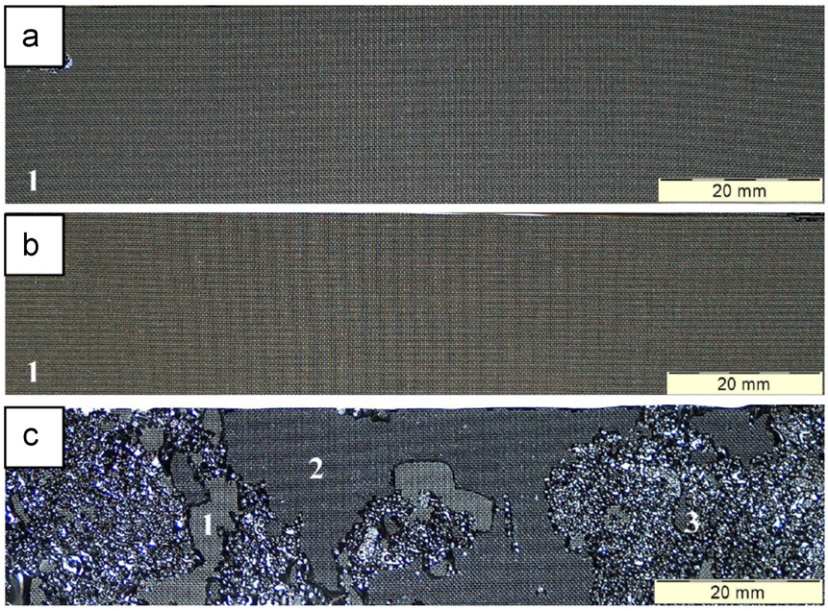

Fig. 9. Macroscopic view of the fracture surfaces of the joints with neat epoxy adhesive (a) and adhesives reinforced with CNFs (b) and CNTs (c). (1) is the surface of the composite, (2) is the surface of the adhesive that was in contact with the substrate (adhesive failure) and (3) is the fracture surface of the adhesive (cohesive failure within the adhesive).

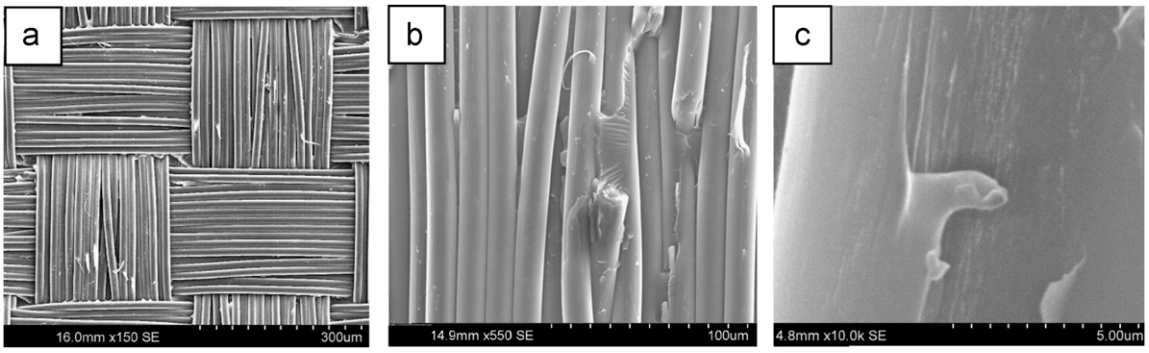

Fig. 10. SEM micrographs of the fracture propagation zone of the joints with neat epoxy adhesive, showing the side with adhesive.

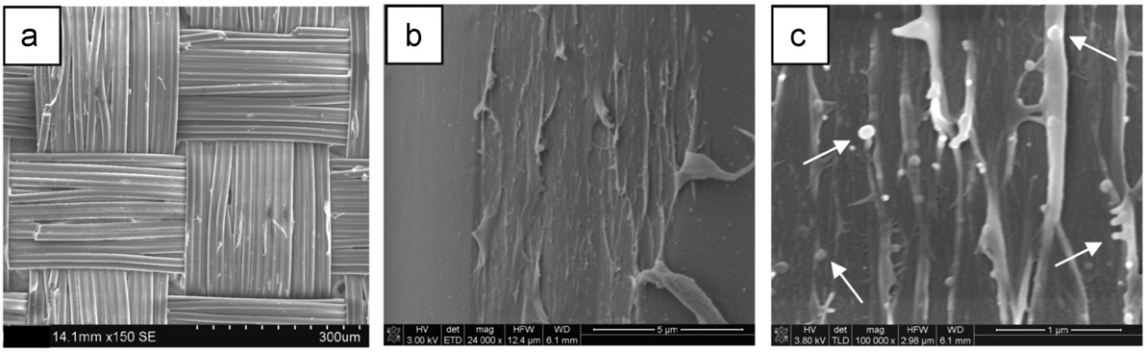

Fig. 11. SEM micrographs of the fracture propagation zone of the joints with CNF/epoxy adhesive, showing the side with adhesive. White arrows indicate possible CNFs participating in the microfibrillation of the adhesive.

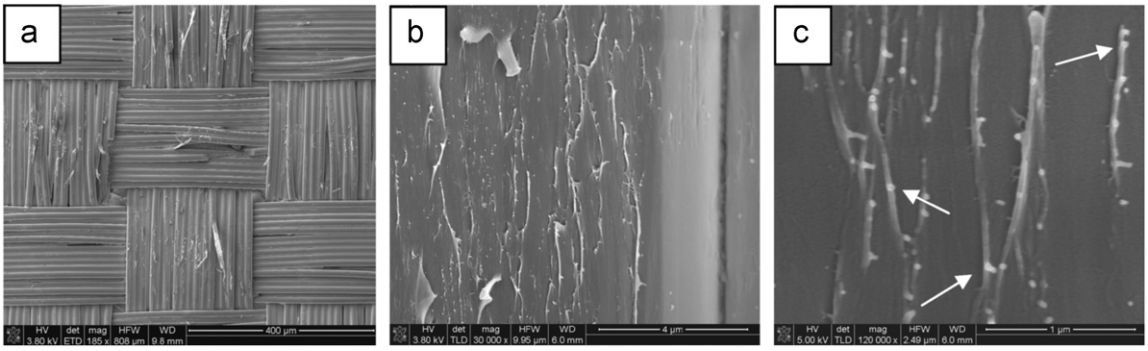

Fig. 12. SEM micrographs of the fracture propagation zone of the joints with CNT/epoxy adhesive, showing the side with adhesive. White arrows indicate possible CNTs participating in the microfibrillation of the adhesive.

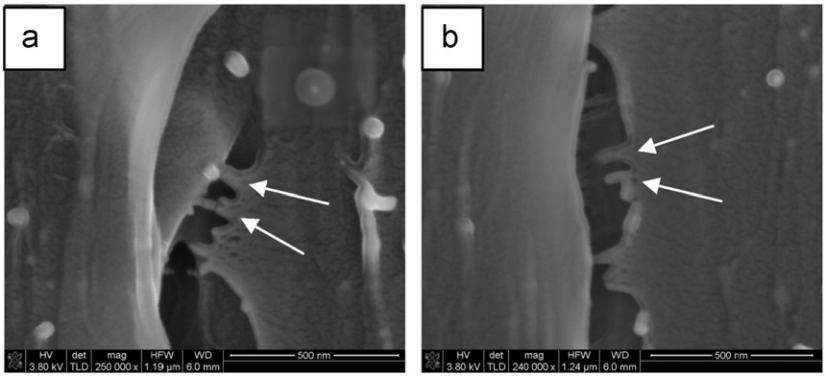

Fig. 13. High-resolution micrographs showing the participation of CNTs, marked with white arrows, in bridging (a) and pull-out micromechanisms (b).

magnification (Figs. 10a, 11a and 12a), we observed the adhesive surface replicating the typical texture left by the peel ply on the adherend surface. In the nanoreinforced adhesives, there were some signs of fibrillation, found more often in the adhesive with CNTs.

Higher magnification observations of the neat adhesive (Fig. 10b and c) showed flat surfaces with a near-total absence of fibrillation, which indicates very low energy consumption during crack propagation. In the nanoreinforced adhesives, there were zones of microcohesive failure, increasing the participation of fibrillation micromechanisms (Figs. 11b and 12b), which were promoted by the presence of CNFs and CNTs, marked with white arrows in Figs. 11c and 12c, respectively. This toughening mechanism explains the slightly higher values of G_{IC} calculated for the adhesive reinforced with CNFs compared with neat adhesive. The CNT/epoxy nanocomposite provided even better adhesive fracture energy due to the presence of additional micromechanical mechanisms such as crack bridging (Fig. 13a) and CNT pull-out (Fig. 13b). As reported by Gojny et al. [8], these are some of the mechanisms leading to increased fracture toughness in epoxy nanocomposites.

4. Conclusions

Peel ply is a surface treatment that, apart from being very easy to apply, provides a very rough surface, significantly increasing the area available for bonding over that of a flat surface. This roughness yields a high dispersive surface energy, and the lack of contaminants and polar groups considerably decreases the polar

component of the surface energy. The total surface free energy is higher than that of untreated laminates, allowing adhesives to better wet adherends treated with peel ply.

Despite this higher roughness and improved wetting over untreated adherends, all tested joints with neat adhesive and peel ply treatment failed in adhesive mode. The lap shear strength obtained with this surface treatment was not influenced by the presence of carbon nanoreinforcements in the adhesive. However, interesting results were obtained in the study of mode-I adhesive fracture energy. Taking into account the standard deviation, the propagation values of G_{IC} remained approximately constant when carbon nanofibres were added to the epoxy adhesive. The slight increase in the mean value could be due to the appearance of microfibrillation, which is a mechanism of energy consumption during fracture that was not present in the neat adhesive. The addition of carbon nanotubes caused an increase in the mode-I adhesive fracture energy associated with microfibrillation and additional toughening mechanisms such as crack bridging and nanotube pull-out. Additionally, in the DCB joints bonded with CNT/epoxy adhesive, there was also a change in the macroscopic failure mode to a mixed adhesive/cohesive failure in the adhesive instead of a completely adhesive failure. A good agreement was also found between the different methods used for the calculation of G_{IC}.

Acknowledgements

The authors would like to acknowledge the financial support from the Ministerio de Ciencia e Innovación of Spain (Project MAT2007-61178) and the Consejería de Educación of Comunidad de Madrid (Programme S2009MAT/1585). María R. Gude also thanks the Consejería de Educación of Comunidad de Madrid and the Fondo Social Europeo for awarding a research contract.

References

[1] Chin JW, Wightman JP. Surface characterization and adhesive bonding of toughened bismaleimide composites. Composites Part A 1996;27A:419–28.
[2] Bénard Q, Fois M, Grisel M. Peel ply surface treatment for composite assemblies: chemistry and morphology effects. Composites Part A 2005;36:1562–8.
[3] Chikhi N, Fellahi S, Bakar M. Modification of epoxy resin using reactive liquid (ATBN) rubber. Eur Polym J 2002;38:251–64.
[4] Kumar P, Tiwari S, Singh RK. Characterization of toughened bonded interface against fracture and impact loads. Int J Adhes Adhes 2005;25:527–33.
[5] Gilbert EN, Hayes BS, Seferis JC. Nano-alumina modified epoxy based film adhesives. Polym Eng Sci 2003;43:1096–104.
[6] Jana S, Zhong W-H, Gan YX. Characterization of the flexural behaviour of a reactive graphitic nanofibers reinforced epoxy using a non-linear damage model. Mater Sci Eng A 2007;445–446:106–12.
[7] Choi Y-K, Sugimoto K-I, Song S-M, Gotoh Y, Ohkoshi Y, Endo M. Mechanical and physical properties of epoxy composites reinforced by vapor grown carbon nanofibers. Carbon 2005;43:2199–208.
[8] Gojny FH, Wichmann MHG, Fiedler B, Schulte K. Influence of different carbon nanotubes on the mechanical properties of epoxy matrix composites—a comparative study. Compos Sci Technol 2005;65:2300–13.
[9] Kim YJ, Shin TS, Choi HD, Kwon JH, Chung Y-C, Yoon HG. Electrical conductivity of chemically modified multiwalled carbon nanotube/epoxy composites. Carbon 2005;43:23–30.
[10] Prolongo SG, Burón M, Gude MR, Chaos-Morán R, Campo M, Ureña A. Effects of dispersion techniques of carbon nanofibers on the thermo-physical properties of epoxy nanocomposites. Compos Sci Technol 2008;68:2722–30.
[11] Prolongo SG, Gude MR, Ureña A. Rheological behaviour of nanoreinforced epoxy adhesives of low electrical resistivity for joining carbon fiber/epoxy laminates, J. Adhes Sci Technol 2010;24:1097–112.
[12] Miyagawa H, Rich MJ, Drzal LT. Thermo-physical properties of epoxy nanocomposites reinforced by carbon nanotubes and vapour grown carbon fibers. Thermochim Acta 2006;442:67–73.
[13] Park J-M, Kim D-S, Kim S-J, Kim P-G, Yoon D-J, DeVries KL. Inherent sensing and interfacial evaluation of carbon nanofiber and nanotube/epoxy composites using electrical resistance measurement and micromechanical technique. Composites Part B 2007;38:847–61.
[14] Prolongo SG, Gude MR, Ureña A. Synthesis and characterisation of epoxy resins reinforced with carbon nanotubes and nanofibers. J Nanosci Nanotechnol 2009;9:6181–7.
[15] Chaos-Morán R, Campo M, Prolongo SG, Escalera MD, Ureña A. The functionalization of carbon nanofibers with 4,4′-diaminodiphenylmethane, a curing agent for epoxy resins. J Mater Res 2009;24:1435–45.
[16] Prolongo SG, Gude MR, Sanchez J, Ureña A. Nanoreinforced epoxy adhesives for aerospace industry. J Adhes 2009;85:180–99.
[17] 〈www.imagemet.com〉.
[18] Kim JK, Lee DG. Characteristics of plasma surface treated composite adhesive joints at high environmental temperature. Compos Struct 2002;57:37–46.
[19] Shanahan MER, Bourgès-Monnier C. Effects of plasma treatment on the adhesion of an epoxy adhesive. Int J Adhes Adhes 1996;16:129–35.
[20] Xu Z, Chen L, Huang Y, Li J, Wu X, Li X, et al. Wettability of carbon fibers modified by acrylic acid and interface properties of carbon fiber/epoxy. Eur Polym J 2008;44:494–503.
[21] Owens DK, Wendt RC. Estimation of the surface free energy of polymers. J Appl Polym Sci 1969;13:1741–7.
[22] Blackman B, Kinloch A. Fracture tests on structural adhesive joints. In: Moore DR, Pavan A, Williams JG, editors. Fracture mechanics testing methods for polymers, adhesives and composites. Oxford: Elsevier; 2001. p. 225–67.
[23] Blackman B, Kinloch AJ, Paraschi M, Teo WS. Measuring the mode I adhesive fracture energy, G_{IC}, of structural adhesive joints: the results of an international round-robin. Int J Adhes Adhes 2003;23:293–305.
[24] Whitney JM, Browning CE, Hoogsteden W. A double cantilever beam test for characterizing mode I delamination of composite materials. J Reinf Plast Compos 1982;1:297–313.
[25] Packham DE. Surface energy, surface topography and adhesion. Int J Adhes Adhes 2003;23:437–48.